Research article

Low-cost zeolite-based sorbents prepared from industrial perlite by-product material for Zn^{2+} and Ni^{2+} removal from aqueous solutions: synthesis, properties and sorption efficiency

Marek Osacký [a],[*], Tomáš Binčík [a], Barbora Hudcová [b], Martina Vítková [b], Helena Pálková [c], Pavol Hudec [d], Peter Bačík [a],[e], Adriana Czímerová [c]

[a] Department of Mineralogy, Petrology and Economic Geology, Comenius University, Mlynská dolina, Ilkovičova 6, 842 15, Bratislava, Slovak Republic
[b] Department of Environmental Geosciences, Czech University of Life Sciences, Kamýcká 129, 165 00, Prague, Czech Republic
[c] Institute of Inorganic Chemistry, Slovak Academy of Sciences, Dúbravská cesta 9, 845 36, Bratislava, Slovak Republic
[d] Department of Organic Technology, Catalysis and Petroleum, Slovak University of Technology, Radlinského 9, 812 37, Bratislava, Slovak Republic
[e] Earth Science Institute, Slovak Academy of Sciences, Dúbravská cesta 9, 840 05, Bratislava, Slovak Republic

HIGHLIGHTS

- Zeolites X and P, phillipsite, analcime, sodalite and cancrinite were synthesized.
- Zeolite content and framework topology affected the metals removal efficiency.
- Zeolite X-based sorbent exhibited the highest metals removal efficiency.

GRAPHICAL ABSTRACT
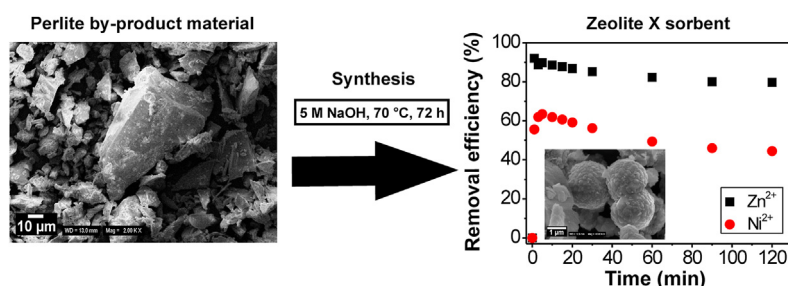
ARTICLE INFO

ABSTRACT

The conversion of waste/by-product materials into efficient sorbents is at the forefront of innovative remediation techniques. In the present study, the relationships among the synthesis conditions, physicochemical properties of synthesized sorbents and Zn^{2+} and Ni^{2+} removal efficiencies were studied in detail. Zeolite X, zeolite P, phillipsite, analcime, sodalite and cancrinite were synthesized from industrial perlite by-product material. The zeolite content in the synthesized sorbents and zeolite framework topology (dimensions, numbers and spatial configuration of channels) were the key factors affecting the removal of Zn^{2+} and Ni^{2+} from aqueous solutions. Zeolite X-based sorbent exhibited the best sorption performance mainly due to the large zeolite channel dimensions, low Si/Al ratio, high cation exchange capacity and high specific surface area. Nevertheless, the efficiency and stability of this sorbent need to be tested under field conditions prior to its application for remediation technologies.

---

* Corresponding author.
  E-mail address: mosacky@hotmail.com (M. Osacký).

1. Introduction

Based on the estimated world crude perlite production for 2018, Slovakia is among the top ten world's leading perlite producers with the annual production of 36 000 tons [1, 2]. Perlite is a hydrated amorphous volcanic glass that expands up to 20 times its original volume when rapidly heated. Commercially, nearly all perlite is used in its expanded form. However, throughout the processing of crude perlite, large quantities of fines (~30 % of the total crude perlite production) are produced as a by-product. Because of small particle size, perlite by-product (PBM) cannot be used for expansion which substantially limits its possible application. The PBM is used only as an additive to Portland cement. Prospective utilization for PBM is the conversion of PBM to zeolites, i.e. value-added materials with exceptional sorption properties. The zeolitization process reduces the accumulation of PBM in future and allows for valorization and recycling of PBM [3].

Zeolites are group of hydrated aluminosilicate minerals of the alkalies and alkaline earths composed of a three-dimensional framework of TO_4 tetrahedra (T = Si, Al). The non-equivalent isomorphous substitution of Al^{3+} for Si^{4+} in the tetrahedra generates a negative charge of the framework. The negative charge is balanced by the presence of cations, mainly Na^+, K^+, Ca^{2+} and Mg^{2+}, located in the channels within the zeolite framework. The exchangeable cations are only loosely held in the channels and are readily replaced by cations from the surrounding environment. The wider the channels, the larger the cation, that can be accommodated in the structure.

Laboratory zeolite synthesis has evolved by duplicating the conditions under which natural zeolites were formed. The conventional hydrothermal zeolite synthesis in laboratory conditions are usually carried out in closed reacting systems (autoclaves) at high pH (>12), high temperatures (>100 °C) and short reaction times (from hours to days) [4, 5]. Zeolites can be synthesized from different precursors including volcanic glasses, aluminosilicates and waste materials [4, 5, 6, 7, 8, 9, 12, 13]. The quantity and type of synthesized reaction products are heavily affected mainly by the nature of precursor material, composition of reaction solution, solid/liquid ratio, synthesis time and temperature [5, 12, 14, 15].

Zeolites have been previously investigated for removal of contaminants from municipal, agricultural and industrial wastewaters because of their unique properties such as high cation exchange capacity and sorption properties, good cation selectivity, good regeneration capability and catalytic properties [4, 6, 7, 8, 9]. Zn and Ni are among the most common metal contaminants present in fresh water from mining areas [10]. The elevated concentrations of metals in water may pose risks to human health because they are persistent in nature, non-biodegradable and tend to accumulate in living organisms [4, 8, 9, 10]. Numerous techniques exist for removal of dissolved metals, including precipitation-filtration, ion exchange, reverse osmosis, solvent extraction, oxidation reduction, membrane separation, phytoremediation [16, 17, 18, 19]. Ion exchange-based techniques are one of the most attractive due to easy handling, especially when efficient and low-cost sorbents are used [16]. Natural and/or synthetic ion exchange-based sorbents such as zeolites are often used to reduce the high concentrations of metals in waters to acceptable levels [4, 5, 8, 9, 11].

The recent environmental trends focus on the (re-)use of various low-cost and waste materials to produce sorbents with high affinity to specific contaminants. Moreover, the utilization of local waste materials to prepare sorbents for contaminant removal meets the current circular economy criteria.

The broad range of synthesis conditions was used in the present study to prepare various types of zeolites. The sorption performance of distinct zeolite species synthesized from PBM for Zn^{2+} and Ni^{2+} was evaluated and compared with commercial natural (clinoptilolite-rich rock) and synthetic zeolites (molecular sieve 13X).

In contrast to previous studies, special attention was devoted in the present paper to a better understanding of relationships among: (i) synthesis conditions, (ii) synthesized materials structure and properties, and (iii) pollutants removal efficiencies. The purity of synthesized sorbent materials is essential parameter determining the quality and utilization. However, the quantity of newly-formed phases originated from wastes/by-products has been rarely reported in the past studies. In the current paper, the XRD full-pattern modelling (RockJock program [20]) was used to determine quantitative mineralogy.

2. Materials and methods

2.1. Starting material and zeolite sorbent synthesis

Perlite by-product material (PBM) provided by LBK PERLIT Ltd. (Lehôtka pod Brehmi, Slovakia) was used as starting material for zeolite sorbents synthesis. The as-received PBM was dried at 60 °C for 48 h and passed through a <63 μm sieve using vibratory sieve shaker Fritsch analysette 3 spartan. In the zeolite synthesis, 20 g of PBM was mixed with 220 mL of 1 and 5 M NaOH solution. The synthesis was performed in the PTFE-lined high-pressure reactor Berghof BR-700 at 70–190 °C for 6–144 h (Table 1). The wide range of synthesis conditions was used in order to synthesize various types of zeolites. After the synthesis, solids were separated from liquids by centrifugation (4500 rpm for 20 min). The solids were washed 10 times by distilled water, dried at 60 °C overnight and passed through a 250 μm sieve. The commercially available sorbent materials of natural zeolitic rock rich in clinoptilolite (Nižný Hrabovec deposit, Slovakia) (CPT) and synthetic molecular sieve rich in zeolite X (13X) were used for comparison in sorption experiments. The mineralogy, chemistry, morphology, surface properties and pore structure characteristics of CPT and 13X are shown in Figs. S1, S2, S3 and Tables 2 and 3.

2.2. Methods

The X-ray diffraction (XRD) patterns were recorded using a Phillips PW1710 diffractometer with Cu Kα radiation and graphite monochromator, operating at 20 mA and 35 kV. Quantitative XRD (QXRD) analysis was carried out using the RockJock11 program [20]. Fourier transform infrared (FTIR) spectra in the mid infrared range (4000–400 cm^{-1}) were measured using Nicolet 6700 spectrometer (Thermo Scientific) by the KBr pressed-disc technique. Scanning electron microscopy (SEM) was performed using a Carl Zeiss EVO 40 H V operated at 20 kV with a Bruker energy dispersive X-ray (EDX) silicon drift detector. Unit-cell parameters were refined with DIFFRACplus TOPAS software using Fundamental Parameters to fit the profile. Starting structural models for each zeolite are listed in Table 4. Cation exchange capacity (CEC) was determined by ammonium acetate method according to Czímerová et al. [21]. The N_2 isotherms were determined on degassed samples (200 °C for 24 h) using Micromeritics ASAP 2400 device. The total specific surface area (S_{BET}) was determined using BET theory. The micropore volume (V_{micro}) and the external specific surface area (S_t) were calculated using the t-plot method with the Harkins-Jura standard isotherm. The total pore volume (V_a) was estimated at a relative pressure of 0.99.

2.3. Sorption experiments

For kinetic sorption experiments, 500 mg of sample mixed with 225 mL of demineralized water was stirred (550 rpm) for 24 h at room temperature. Single-metal solutions, with Zn^{2+} and Ni^{2+} concentration of 10^{-3} M, were prepared by dissolution of $ZnCl_2$ and $NiCl_2.6H_2O$ in demineralized water, respectively. Afterward, 25 mL of 10^{-3} M solution of Zn^{2+} and Ni^{2+}, respectively, was added into the sample/demineralized water mixture to maintain the solid/liquid ratio of 2 g L^{-1} and the final concentration of Zn^{2+} and Ni^{2+} of 10^{-4} M. All kinetic sorption experiments were performed at pH 5. After given time intervals (1, 3, 5, 10, 15, 20, 30, 60, 90 and 120 min), 10 mL of suspension was sampled, filtered (cellulose acetate membrane, 0.45 μm pore size) and subsequently

Table 1. Experimental conditions and reaction products synthesized from perlite-by product material (PBM) in NaOH solution.

Sample	PBM initial mass (g)	Solid mass after synthesis (g)	NaOH solution	Time (h)	Temperature (°C)	Products
1-70-72	20.0	18.0	1 M	72	70	–
1-130-24	20.0	16.1	1 M	24	130	Ph
1-130-72	20.0	16.2	1 M	72	130	Ph
1-130-144	20.0	16.0	1 M	144	130	Ph, A
1-190-6	20.0	15.3	1 M	6	190	A, Ph
5-70-72	20.0	10.8	5 M	72	70	X, P, S
5-100-72	20.0	10.4	5 M	72	100	P, S, C
5-100-132	20.0	10.1	5 M	132	100	P, S, C
5-130-24	20.0	9.5	5 M	24	130	C, S
5-190-6	20.0	9.9	5 M	6	190	C
5-80-24	20.0	11.0	5 M	24	80	X, P, S
5-80-72	20.0	10.7	5 M	72	80	P, X, S
5-80-144	20.0	10.4	5 M	144	80	P, X, S

Ph – phillipsite, A – analcime, X – zeolite X, P – zeolite P, S – sodalite, C – cancrinite.

Table 2. SEM-EDX elemental composition (in at%) for starting PBM, synthesized zeolitic materials and commercial sorbents.

Sample	Mineral phase analyzed	O	Si	Al	Na	K	Fe	Ca	Mg	Si/Al
PBM	unaltered volcanic glass	72.52	19.18	4.18	1.30	1.77	0.63	0.33	0.09	4.59
5-70-72	altered volcanic glass	75.52	16.41	4.26	1.69	1.10	0.54	0.36	0.12	3.85
1-130-72	phillipsite	71.50	15.76	7.27	2.73	1.43	0.80	0.41	0.11	2.17
1-190-6	phillipsite	67.90	20.77	7.41	1.60	0.73	1.07	0.34	0.19	2.80
1-190-6	analcime	73.13	14.84	5.81	3.64	1.25	0.70	0.52	0.13	2.55
5-70-72	zeolite X	79.72	8.09	5.97	3.89	0.46	1.26	0.57	0.05	1.36
5-80-72	zeolite X	72.26	10.87	8.74	6.49	0.36	0.88	0.37	0.04	1.24
5-80-72	zeolite P	72.12	12.48	8.55	4.68	0.51	0.96	0.63	0.07	1.46
5-100-132	zeolite P	71.34	12.31	10.70	4.47	0.20	0.67	0.21	0.09	1.15
5-100-132	sodalite	58.65	16.14	15.86	6.64	0.27	0.97	1.22	0.26	1.02
5-190-6	cancrinite	68.66	10.92	9.75	9.00	0.14	0.99	0.42	0.12	1.12
13X	zeolite X	70.09	12.58	11.62	4.52	0.12	0.41	0.58	0.07	1.08
CPT	clinoptilolite	66.53	20.25	7.57	2.45	0.70	0.48	1.91	0.16	2.68

Table 3. Pore structure characteristics and cation exchange capacity for starting PBM, synthesized zeolitic materials and commercial sorbents.

Sample	S_{BET} (m²/g)	S_t (m²/g)	%S_{micro} (%)	V_a (cm³/g)	V_{micro} (cm³/g)	CEC_{AmAc} (meq/100g)	$CEC_{AmAcCorr}$ (meq/100g)
PBM	3.3	2.6	–	0.010	0.000	5 ± 0	5 ± 0
1-130-72	13.3	12.0	–	0.075	0.000	321 ± 9	285 ± 13
1-190-6	10.0	9.4	–	0.056	0.000	200 ± 7	173 ± 7
5-70-72	313	36.9	88.2	0.260	0.145	314 ± 5	261 ± 6
5-80-72	140	21.6	84.6	0.155	0.062	363 ± 1	312 ± 1
5-190-6	16.7	15.5	–	0.096	0.000	274 ± 1	202 ± 10
13X	585	34.4	94.1	0.327	0.289	355 ± 5	344 ± 5
CPT	25.0	20.4	18.4	0.143	0.002	137 ± 3	126 ± 2

S_{BET} – total specific surface area; S_t – specific surface area from mesopores, macropores and external specific surface area obtained from the *t*-plot; %S_{micro} – specific surface area contributed by micropores; V_a – total pore volume; V_{micro} – micropore volume; CEC_{AmAc} – cation exchange capacity determined by ammonium acetate method; $CEC_{AmAcCorr}$ – CEC_{AmAc} corrected for the presence of non-exchangeable cations.

analyzed by ICP-OES (Agilent Technologies 700 Series). The Ni^{2+} and Zn^{2+} removal efficiency (in %) was calculated by the difference in metal concentration in the solution before and after sorption onto studied sample. The kinetic sorption data were modeled by the non-linear form of the pseudo-first order and pseudo-second order [22]. For equilibrium sorption experiments, solutions with Ni^{2+} and Zn^{2+} concentrations ranging from 0.1 to 10 mg L^{-1} were prepared. Individual batches with the solutions at given concentrations and the solid/liquid ratio (2 g L^{-1}) were shaken using an orbital shaker (GFL 3005; 250 rpm) for 120 min, sampled, filtered and analyzed as described previously for kinetic experiments. All equilibrium sorption experiments were performed at pH 5.

The equilibrium sorption data were modeled by the non-linear form of the Freundlich and Langmuir model [23, 24].

3. Results and discussion

3.1. X-ray diffraction (XRD)

The starting perlite by-product material (PBM) consisted mainly of volcanic glass (94 wt%) and accessory minerals such as feldspars (3 wt%), biotite (1 wt%), quartz (1 wt%) and sometimes opal-CT (1 wt%) (Figure 1 and Table 5). After synthesis, the XRD results (Table 5) revealed

Table 4. Unit-cell parameters for zeolites synthesized from PBM.

Sample	Mineral	a [Å]	b [Å]	c [Å]	β [°]	V [Å³]
1-130-72	phillipsite	9.968 (4)	14.180 (8)	8.683 (7)	124.96 (5)	1005.9 (13)
1-190-6	phillipsite	9.970 (5)	14.210 (9)	8.672 (7)	124.88 (5)	1007.9 (13)
Gatta et al. [28]	phillipsite	9.9238	14.3145	8.7416	124.92	1018.201
1-190-6	analcime	13.694 (4)				2568 (2)
Gatta et al. [29]	analcime	13.7065				2575.015
5-70-72	zeolite X	24.98 (2)				15590 (31)
5-80-72	zeolite X	25.03 (1)				15688 (23)
Porcher et al. [30]	faujasite	25.104				15820.812
5-80-72	zeolite P	10.045 (1)	10.130 (5)	9.895 (5)	90.58 (4)	1006.8 (8)
5-100-132	zeolite P	10.132 (6)	10.008 (6)	10.054 (7)	90.34 (13)	1019.4 (11)
Fischer [31]	gismondine	10.02	10.62	9.84	92.42	1046.164
5-100-132	sodalite	8.8647 (15)				696.6 (4)
Hassan et al. [32]	sodalite	8.88696				701.875
5-190-6	cancrinite	12.7652 (14)		5.2075 (9)		734.9 (2)
Hassan et al. [33]	cancrinite	12.590		5.117		702.421

a variable decrease in the amount of volcanic glass (depending on the synthesis conditions). The mass of all synthesized solids was lower than the mass of initial solids mainly due to volcanic glass dissolution (Tables 1 and 5). As expected, more pronounced reduction in solid mass was determined in 5 M NaOH (mass reduction by 45–53 %, Table 1) than in 1 M NaOH (mass reduction by 10–24 %, Table 1).

The main reaction products identified by XRD were zeolite X, zeolite P, phillipsite, analcime, sodalite and cancrinite (Figure 1). The type and quantity of newly-formed zeolites were heavily affected by synthesis conditions. Generally, the concentration (1 M versus 5 M) of NaOH solution had significant impact on the type of synthesized zeolites whereas the reaction temperature and time influenced mainly the quantity of
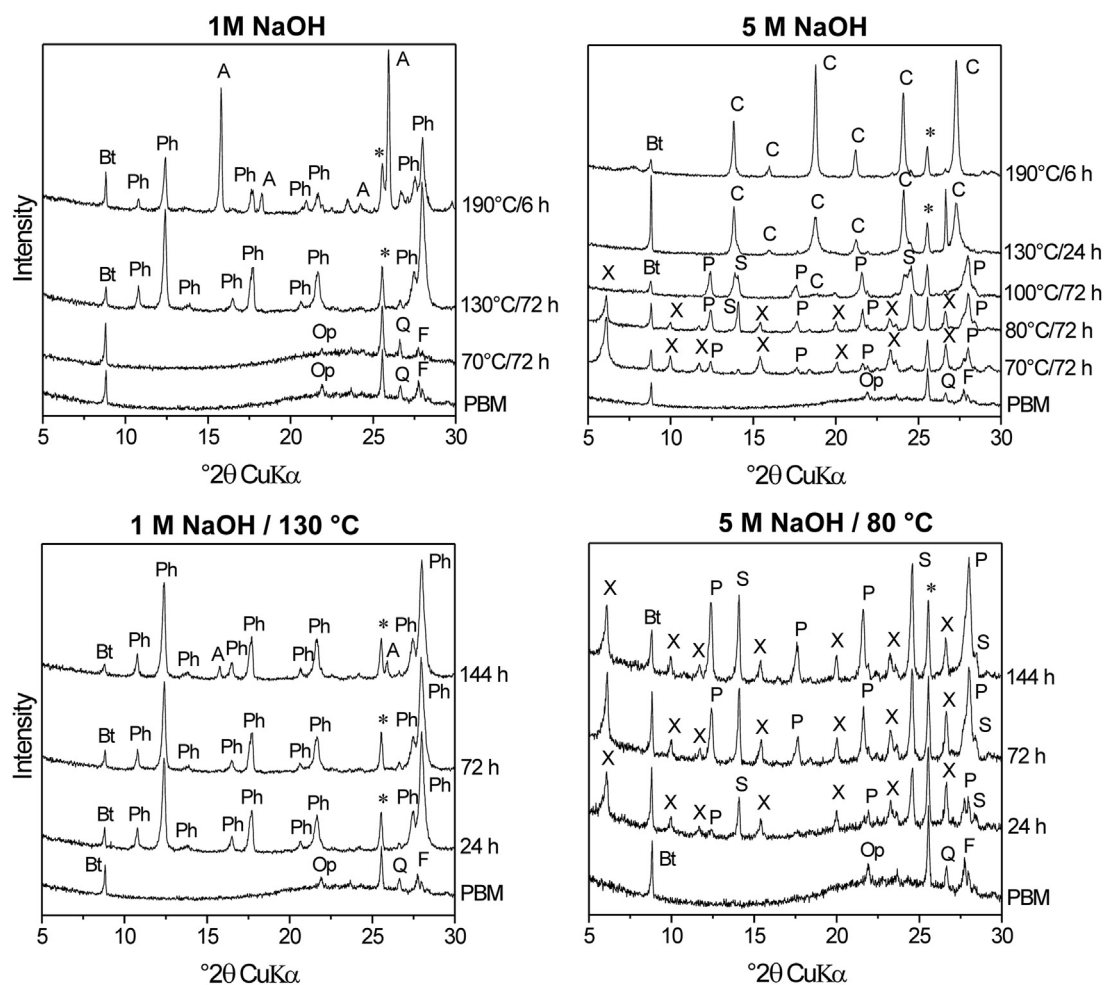

Figure 1. XRD patterns of random preparations for starting PBM and synthesized zeolitic materials. Bt – biotite, Ph – phillipsite, A – analcime, Op – opal-CT, Q – quartz, F – feldspars, C – cancrinite, X – zeolite X, P – zeolite P, S – sodalite, * – corundum (internal standard).

Table 5. Mineral composition (in wt%) for starting PBM and synthesized zeolitic materials determined by RockJock software.

Sample	Volcanic glass	Biotite	Feldspars	Quartz	Opal-CT	Zeolite X	Zeolite P	Phillipsite	Sodalite	Analcime	Cancrinite	Σ Zeolites
PBM	94	1	3	1	1							0
1-70-72	96	1	<1	<1	<1							0
1-130-24	21	3	6		3			67				67
1-130-72	21	4	6	<1	2			66				66
1-130-144	13	3	8		3			70		3		73
1-190-6	10	3	17					33		37		70
5-70-72	42	4	2			38	13		1			52
5-100-72	34	7	6				42		10		<1	53
5-100-132	29	7	2				54		7		<1	62
*5-190-6	13	6	3		3						75	75
5-80-24	69	4	2		<1	15	6		4			25
5-80-72	33	5	5			20	29		9			58
5-80-144	26	4	7			14	38		11			63

* determined using BGMN software.

synthesized zeolite species (Figure 2). Phillipsite and analcime were preferably formed in 1 M NaOH solution while zeolite P, zeolite X, sodalite and cancrinite were preferentially formed in 5 M NaOH (Figure 1).

The high amounts of phillipsite (66–70 wt%) were synthesized from PBM in 1 M NaOH at 130 °C after 24, 72 and 144 h (1-130-24, 1-130-72,

1-130-144, Table 5). After longer reaction time (144 h), phillipsite content was slightly higher (70 wt%) than that after shorter reaction time (66 and 67 wt% of phillipsite after 72 and 24 h, respectively, Table 5). Small amount of analcime (3 wt%) accompanied phillipsite (70 wt%) after synthesis in 1 M NaOH at 130 °C for 144 h (1-130-144, Table 5). The
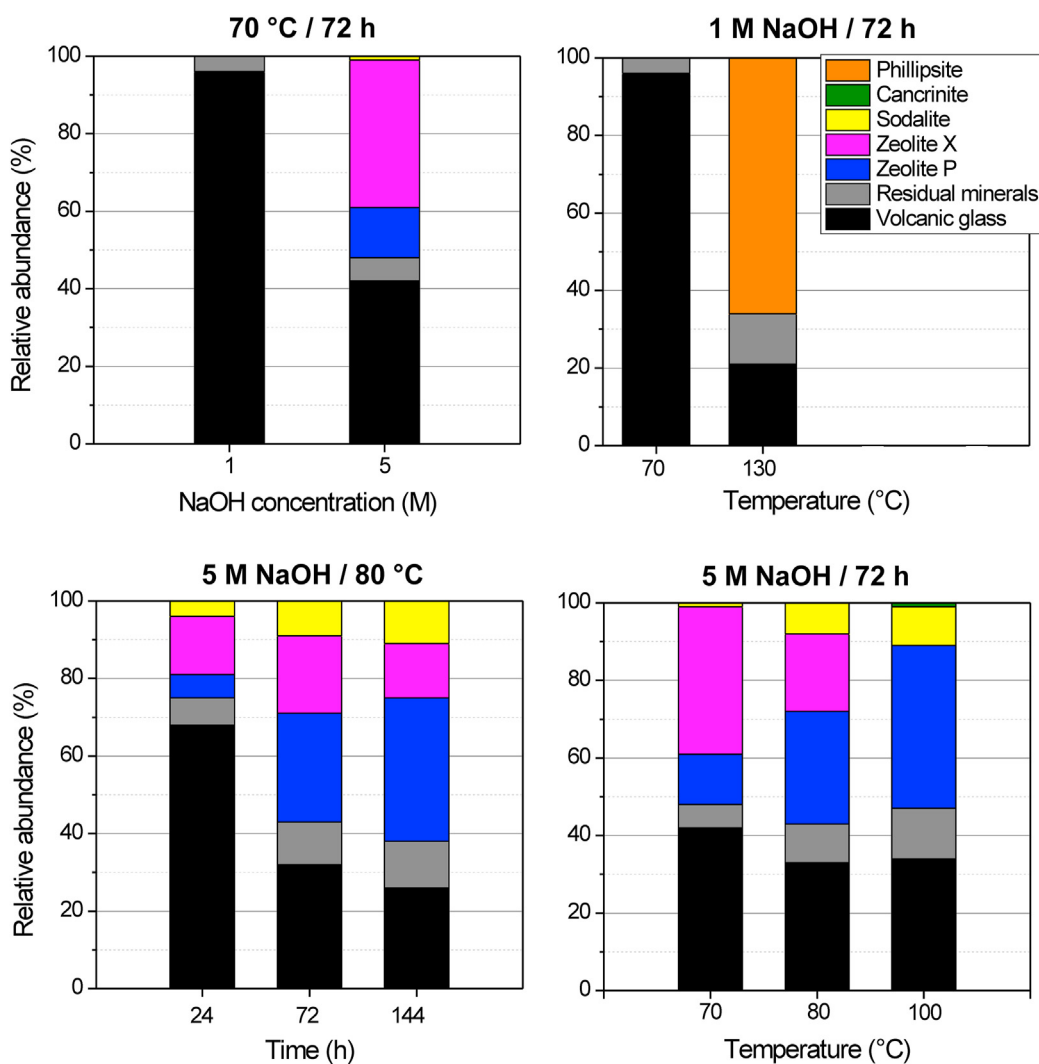

Figure 2. Impact of NaOH concentration, temperature and time on mineralogy of synthesized zeolitic materials. Residual minerals – sum of biotite, feldspars, quartz and opal-CT.

amount of analcime was substantially higher (37 wt%) and the amount of phillipsite was substantially lower (33 wt%) after reaction in 1 M NaOH at 190 °C for 6 h (1-190-6, Table 5).

The reaction of PBM with 5 M NaOH resulted in formation of variable amount of zeolite P (6–54 wt%), zeolite X (0–38 wt%) and sodalite (1–11 wt%) in mutual mixture (Table 5). Zeolite P was formed under wide range of experimental synthesis conditions (70–100 °C, 24–144 h), but its highest amounts (42–54 wt%) were determined for synthesis temperatures of 100 °C (Table 5). At higher temperatures (≥130 °C), no zeolite P was detected by XRD in studied samples (Figure 1). At the synthesis temperatures of 80 and 100 °C, the amount of zeolite P gradually increased with longer reaction time (compare 5-100-72 versus 5-100-132 and 5-80-24 versus 5-80-72 versus 5-80-144, Table 5). Zeolite X, on the other hand, was preferentially formed at lower synthesis temperatures (70–80 °C) than zeolite P. No zeolite X was detected by XRD in 5 M NaOH at elevated temperatures (≥100 °C) within the studied experimental conditions (Table 5 and Figure 1). The largest amount of zeolite X (38 wt%), accompanied with zeolite P (13 wt%) and traces of sodalite (1 wt%), was synthesized from PBM in 5 M NaOH at 70 °C after 72 h (5-70-72, Table 5). At slightly higher temperature (80 °C), lower amount of zeolite X (14–20 wt%) accompanied with variable amount of zeolite P (6–38 wt%) and sodalite (4–11 wt%) was formed from PBM in 5 M NaOH after 24–144 h (5-80-24, 5-80-72 and 5-80-144, Table 5). Sodalite was synthesized from PBM treated with 5 M NaOH solution under wide range of experimental conditions (70–130 °C, 24–144 h). However, in all cases, sodalite occurred as a minor mineral constituent accompanying the main reaction products, mainly zeolite X and zeolite P, sometimes cancrinite (Table 5). Cancrinite was identified by XRD in PBM treated with 5 M NaOH at temperatures ranging from 100 to 190 °C. Increasing XRD intensity of cancrinite reflections with synthesis temperature (Figure 1) indicated gradual increase in relative amount of cancrinite with increasing temperature. At 100–130 °C, cancrinite was in association with sodalite and zeolite P. At the temperature of 190 °C, cancrinite was the only reaction product synthesized from PBM (75 wt% of cancrinite for 5-190-6, Table 5 and Figure 1).

3.2. Fourier transform infrared spectroscopy (FTIR)

The PBM showed FTIR spectra typical for volcanic glass. The prominent band at 1042 cm^{-1} was attributed to the asymmetric stretching Si–O vibration (Figure 3a). The absorption bands at 787 and 465 cm^{-1} were assigned to the symmetric stretching Si–O vibration and bending Si–O–Si vibration, respectively.

FTIR spectra of all zeolitic materials synthesized from PBM displayed the prominent band in the 1032–984 cm^{-1} region, corresponding to the asymmetric stretching vibration of TO$_4$ tetrahedra (T = Si, Al) in zeolites. Samples reacted with 1 M NaOH solution (1-130-72, 1-190-6, Fig. 3b, c) showed the maxima of this band between 1032 and 1024 cm^{-1} whereas samples reacted with 5 M NaOH (5-70-72, 5-80-72 and 5-190-6, Fig. 3d-f) showed the maxima at 997–984 cm^{-1}. The shift of the asymmetric stretching TO$_4$ vibration towards lower wavenumbers with increasing concentration of NaOH solution may be due to the increase in the proportion of tetrahedral Al in the structure of synthesized zeolites. This conjecture was confirmed by chemical composition (Si/Al ratio) of synthesized zeolites (Table 2) and was in line with published data [14, 15]. The bending vibrations of TO$_4$ in synthesized zeolites were observed approximately between 470 and 425 cm^{-1}.

The absorption bands in the range of 800–500 cm^{-1} were due to the pseudolattice vibrations of zeolites originating from overtetrahedral structural units (rings made of SiO$_4$ and AlO$_4$ tetrahedra) [15]. The absorption bands characteristic of cancrinite (near 681, 624 and 568 cm^{-1} [25]) were observed in the FTIR spectrum of cancrinite rich sample 5-190-6 (Figure 3f). An inflection near 1441 cm^{-1} (stretching CO$_3^{2-}$ vibration) observed in the same FTIR spectrum was due to carbonate groups likely located in the large open cancrinite channels [25, 26].
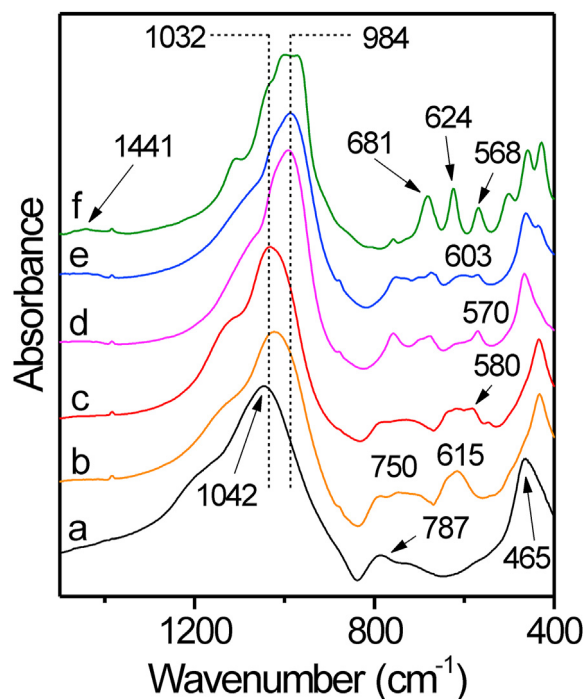

Figure 3. FTIR spectra for starting PBM (a), 1-130-72 (b), 1-190-6 (c), 5-70-72 (d), 5-80-72 (e) and 5-190-6 (f).

The presence of phillipsite in the synthesized materials (1-130-72 and 1-190-6, Fig. 3b, c) was indicated by absorption near 615 cm^{-1} [14,26]. The comparison of FTIR spectra for 1-130-72 (Figure 3b) and 1-190-6 (Figure 3c) revealed that the intensity of the ~615 cm^{-1} band decreased with decreasing amount of phillipsite which was in line with QXRD results (Table 5). An inflection near 580 cm^{-1} in the FTIR spectrum of 1-190-6 (Figure 3c) may be due to the symmetric mode of TO$_4$ vibration of analcime [13]. The FTIR spectra of zeolite X rich samples 5-70-72 Figure 3d) and 5-80-72 (Figure 3e) was similar to that of commercial molecular sieve 13X consisting of pure zeolite X (Fig. S2). The QXRD results (Table 5) along with published data [14] showed that the intensity of the 570 cm^{-1} band increased with increasing amount of zeolite X in the samples.

3.3. Scanning electron microscopy (SEM)

The starting PBM consisted predominantly of volcanic glass grains, typically between 10 and 60 μm in size (Figure 4a). After reaction of PBM with NaOH, micrometer-sized hemispherical etch pits were observed on the surface of volcanic glass particles as a result of volcanic glass dissolution (Figure 4b). Phillipsite (1-130-72) occurred in the form of intergrown (rarely individual) spherical particles (~5–10 μm in diameter) consisting of a large number of well-developed prismatic crystals, typically up to 1 μm in length (Figure 4c). Analcime (1-190-6) displayed easily recognizable large (several 10's to ~50 μm in diameter) rounded particles of characteristic trapezohedral morphology (Figure 4d). The surface of analcime crystals was not cleanly facetted but exhibited many intergrowths. Zeolite X (5-70-72) showed rounded aggregates ranging in sizes from 2 to 5 μm composed of a large number of well-developed fine zeolite X crystals with sharp edges which often had octahedral morphology (Figure 4e). Such octahedral morphology is typical for FAU-type zeolites [27]. Zeolite P (5-100-132) formed well-developed euhedral tabular crystals which were often in a radial arrangement forming aggregates (up to 5–6 μm in diameter) with a flower-like external geometry (Figure 4f). Cancrinite (5-190-6) formed aggregates of different sizes and shapes composed of randomly oriented laths and needles up to 2 μm long (Figure 4g). Sodalite (5-100-132) was
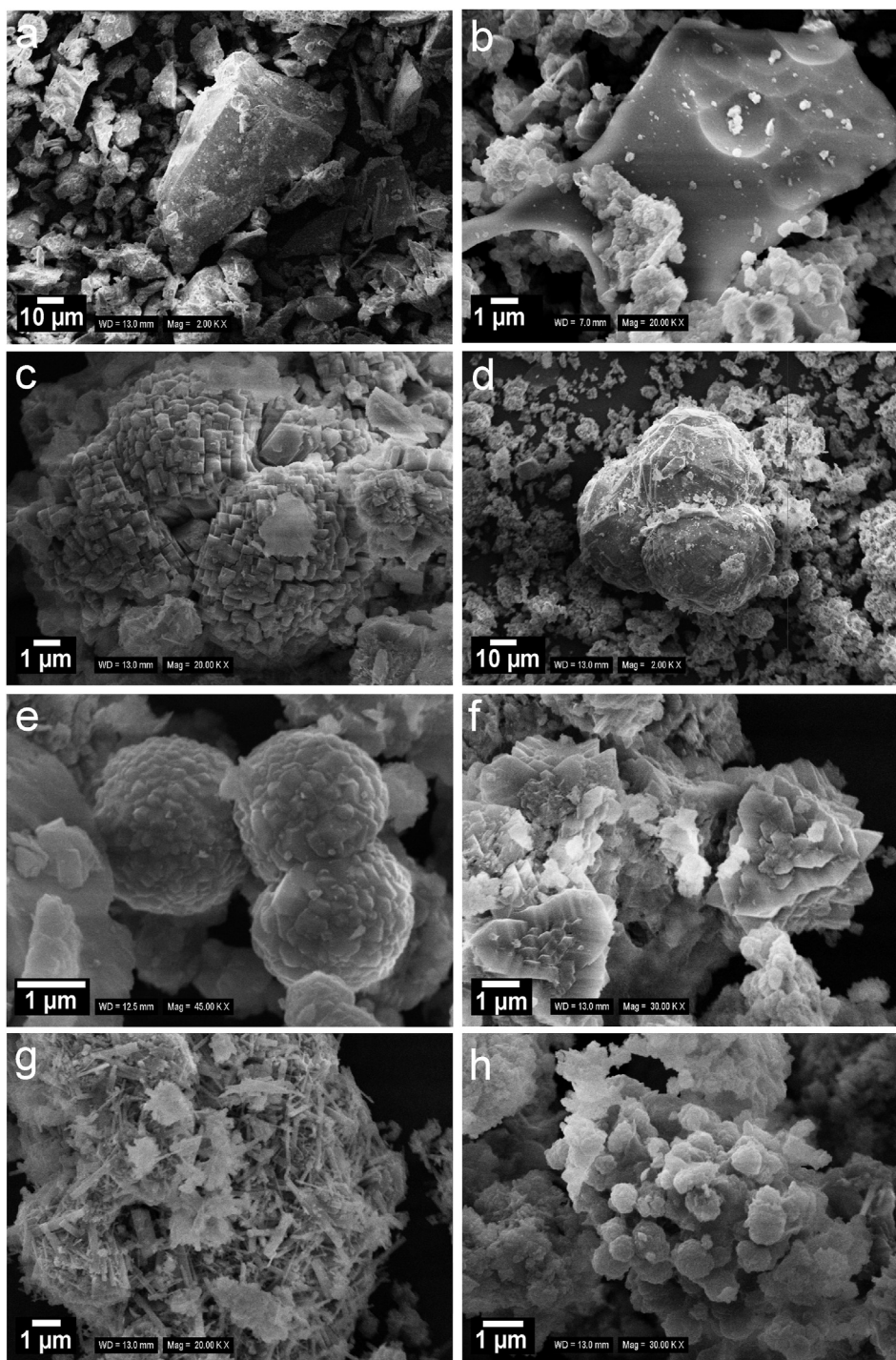
Figure 4. SEM images of starting volcanic glass (a), reacted volcanic glass (b), phillipsite (c), analcime (d), zeolite X (e), zeolite P (f), cancrinite (g) and sodalite (h).

observed in the form of spherical cauliflower-like aggregates (<1 μm in diameter) (Figure 4h).

3.4. Energy dispersive X-ray spectroscopy (EDX) and unit-cell parameters refinement

The EDX analyses of volcanic glass and synthesized zeolites are reported in Table 2. The EDX results of volcanic glass before (Si/Al = 4.59, Table 2) and after (Si/Al = 3.85, Table 2) reaction with NaOH showed lower Si/Al ratio for altered volcanic glass particles after NaOH interaction compared to those before NaOH interaction. Volcanic glass particles reacted with NaOH solutions were depleted mainly in Si due to

volcanic glass dissolution. Figure 5 shows the main differences in chemistry among different types of zeolites synthesized from PBM. Zeolites formed in 5 M NaOH (zeolite X, zeolite P, sodalite and cancrinite) were distributed in low Si (Si/Al ratio <1.5) and higher Na (Na/Na + K + Ca + Mg + Fe ratio >0.75) region whereas the zeolites formed in 1 M NaOH (analcime and phillipsite) were distributed in high Si (Si/Al ratio >2.1) and lower Na (Na/Na + K + Ca + Mg + Fe ratio <0.75) region.

The calculated unit-cell parameters of phillipsites synthesized from PBM (1-130-72 and 1-190-6) were slightly lower than those of natural phillipsite from Richmond, Victoria, Australia [28] except *a* (Table 4). This may be related to the different Si/Al ratios between the synthesized phillipsites 1-130-72 and 1-190-6 (Si/Al = 2.17 and 2.80, Table 2) and
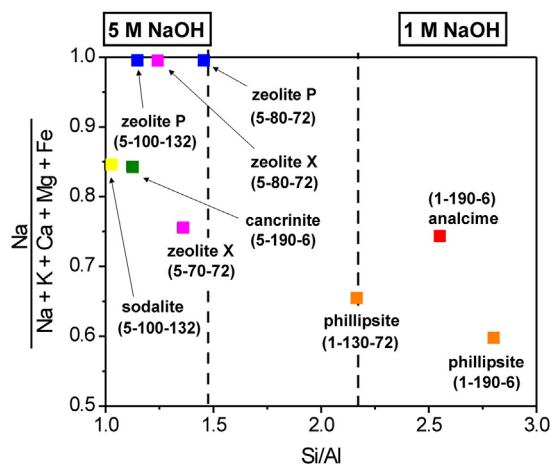
Figure 5. The chemical composition of zeolites synthesized from PBM in 1 M and 5 M NaOH solution.

the natural phillipsite from Richmond, Victoria, Australia (Si/Al = 1.67 [28]). Consequently, the synthesized phillipsites with higher Si content had more compressed unit cells. The variations in unit-cell parameters among the three analyzed phillipsites (Table 4) may be due to the different ordering of Al and Si atoms at the tetrahedral sites. Synthesized analcime (1-190-6) was refined in a cubic symmetry and was very similar to the natural cubic analcime [29] (Table 4). Small variations in unit-cell parameters among the synthesized zeolites X (5-70-72 and 5-80-72) and faujasite (natural equivalent of zeolite X) [30] (Table 4) were related to the distinct Si/Al ratio; with higher Si content the unit-cell parameters were smaller. The same relationship (smaller unit-cell parameters with higher Si content) was observed for zeolites P (5-80-72 and 5-100-132) and gismondine (natural equivalent of zeolite P) [31]. However, small variations of unit-cell parameters in monoclinic zeolites P and gismondine can be also attributed to the differences in Al and Si ordering. A slightly higher Si/Al ratio for synthesized sodalite (5-100-132) may be related to the negligible compression of the unit cell compared to the natural sodalite [32]. On the other hand, the larger unit cell of synthesized cancrinite (5-190-6) compared to the natural cancrinite [33] may be associated with the higher amount of Fe incorporated into the structure of synthetic cancrinite 5-190-6. The experimental conditions (e.g. synthesis temperature and time) may have also some impact on the Si/Al ratio and ordering of these atoms at the tetrahedral site of synthesized zeolites.

3.5. Cation exchange capacity (CEC)

After zeolite synthesis, all solid products were washed 10 times by distilled water in order to remove the excess of NaOH from the samples. However, it is possible that certain amount of leachable (i.e. non-exchangeable) cations (in particular Na^+ derived from residual NaOH) resisted the intensive washing by distilled water. The non-exchangeable cations may be erroneously attributed to ion exchange processes (i.e. to exchangeable cations located in the channels and cages within the zeolite framework) which may overestimate the measured CEC_{AmAc} values (i.e. CECs determined by ammonium acetate method) (Table 3). In order to distinguish between the exchangeable and non-exchangeable cations for the studied samples the CEC procedure was repeated in the same way but using Millipore deionized water instead of ammonium acetate solution. The cations released from the studied samples into Millipore deionized water were attributed to the non-exchangeable cations located outside the open structural cavities (channels and cages) of zeolites (e.g. in interparticle or interaggregate pores).

The CEC_{AmAc} values were then corrected for the presence of non-exchangeable cations and the corrected CEC values ($CEC_{AmAcCorr}$) are

reported in Table 3. The comparison of the CEC_{AmAc} and the $CEC_{AmAcCorr}$ values for the synthesized zeolitic materials showed an overestimation of the CEC_{AmAc} values by 11–26 %. The Na^+, Ca^{2+}, Mg^{2+}, K^+ and Fe^{3+} were the main non-exchangeable cations derived from synthesized zeolitic materials. As expected, the levels of released non-exchangeable Na^+ (20–54 meq Na^+/100g, Table S1) greatly exceeded the sum of other non-exchangeable cations (3–14 meq $Ca^{2+} + Mg^{2+} + K^+ + Fe^{3+}$/100g, Table S1). Zeolitic materials synthesized from PBM in 5 M NaOH solution released substantially higher levels of non-exchangeable Na^+ (44–54 meq Na^+/100g, Table S1) than those synthesized from PBM in 1 M NaOH (20–29 meq Na^+/100g, Table S1).

The $CEC_{AmAcCorr}$ depended mainly on the quantity and type of zeolites present in the studied samples. The highest $CEC_{AmAcCorr}$ (312 ± 1 meq/100g, Table 3) of synthesized materials displayed the sample 5-80-72, containing 29 wt% of zeolite P and 20 wt% of zeolite X. The sample 1-130-72 with 67 wt% of phillipsite had $CEC_{AmAcCorr}$ of 285 ± 13 meq/100g (Table 3). The sample 5-70-72 containing 38 wt% of zeolite X and 13 wt% of zeolite P had the $CEC_{AmAcCorr}$ of 261 ± 6 meq/100g (Table 3). The synthesized material 5-190-6 rich in cancrinite (75 wt%) had the $CEC_{AmAcCorr}$ of 202 ± 10 meq/100g (Table 3). The lowest $CEC_{AmAcCorr}$ (173 ± 7 meq/100g, Table 3) was determined for synthesized material 1-190-6 consisting of analcime (37 wt%) and phillipsite (33 wt%).

3.6. Textural properties

The isotherm shape of PBM (type II isotherm [34]) (Figure 6a) showed an extremely low amount of gas adsorption for the entire relative pressure (P/P_0) range which is characteristic for non-porous or macro-porous (diameter >50 nm) material [34]. PBM had the lowest total pore volume ($V_a = 0.01$ cm^3/g) and total specific surface area ($S_{BET} = 3.3$ m^2/g) of all studied samples (Table 3). The isotherms of zeolitic materials synthesized from PBM showed larger gas adsorption and more pronounced hysteresis loop. Generally, a purely microporous (diameter <2 nm) adsorbent exhibits a concave shape isotherm with very high gas adsorption at very low relative pressure ($P/P_0 < 0.01$) while a purely mesoporous material has a hysteresis loop which is associated with capillary condensation in mesopores (diameter 2–50 nm) [34].

The synthesized materials rich in zeolite X (5-70-72) and zeolite P + zeolite X (5-80-72) showed type I isotherms [34] with high amount of gas adsorbed at very low relative pressure ($P/P_0 < 0.01$) which suggested a higher proportion of micropores in these particular samples compared to the rest of the synthesized materials. This conjecture was in line with the pore structure characteristics determined for studied materials (Table 3). The results showed that the micropores ($\%S_{micro}$) accounted for ~85 % and ~88 % of the total specific surface area (S_{BET}) in the samples 5-80-72 and 5-70-72, respectively (Table 3). The synthesized materials rich in zeolite X (5-70-72) and zeolite P + zeolite X (5-80-72) had substantially higher total pore volume ($V_a = 0.155$–0.260 cm^3/g) and total specific surface area ($S_{BET} = 140$–313 m^2/g) than synthesized materials rich in phillipsite (1-130-72), analcime + phillipsite (1-190-6) and cancrinite (5-190-6) ($V_a = 0.056$–0.096 cm^3/g and $S_{BET} = 10$–16.7 m^2/g) (Table 3).

The pore-size distribution (PSD) (Figure 6b) for synthesized material rich in cancrinite (5-190-6) showed one sharp and very intense peak around 100 nm. The rest of the studied samples showed a broad shoulder between 10 and 200 nm with the maxima pore volume around 80 nm for phillipsite (1-130-72) and analcime + phillipsite (1-190-6) rich samples and with the maxima pore volume around 25 nm for zeolite X (5-70-72) and zeolite P + zeolite X (5-80-72) rich samples.

3.7. Sorption efficiency

The sorption efficiencies of synthesized zeolitic materials and commercial sorbents at pH 5 for Zn^{2+} and Ni^{2+} are illustrated in Figure 7. For the sorption of Zn^{2+} and Ni^{2+}, the equilibrium time was reached after 60 min for all tested materials. Within the first 60 min, approximately 15 and 19 % of Ni^{2+} sorbed onto 5-70-72 and 13X, respectively, was
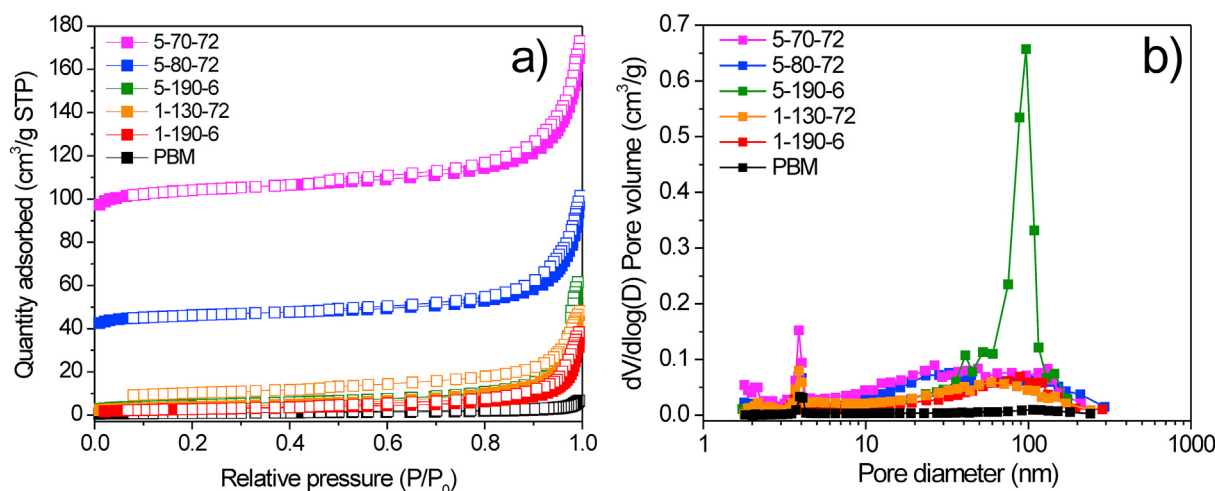
Figure 6. Adsorption-desorption N_2 isotherms (a) and pore-size distributions (b) for starting PBM and synthesized zeolitic materials.

desorbed into the solution and afterwards the sorbed amount was equilibrated. Similarly, about 10 % of Zn^{2+} was desorbed from the 5-70-72 into the solution under the same experimental conditions. At the same time, as desorption was taking place, the Al^{3+} ions leached from the zeolitic framework were removed from the solution, indicating their possible resorption onto 5-70-72 and 13X (Fig. S4). These results indicated that the presence of competing cations with relatively low hydration energies and high charges (i.e. Al^{3+}) decreased the sorption efficiency of studied materials for Ni^{2+} and Zn^{2+}. Our results also showed that the presence of competing cations in solution had more detrimental effect on the sorption of Ni^{2+} than Zn^{2+}. Based on EDX results (Table 2) the main sources of Al^{3+} in the solutions were: (i) zeolites, more specifically the Al^{3+} released from the exchangeable sites located within the zeolite framework, and/or (ii) volcanic glass, more specifically the Al^{3+} leached from volcanic glass structure after reaction with NaOH due to glass dissolution. The "free" Al^{3+} remaining in a sample after zeolite synthesis (i.e. Al^{3+} not incorporated into the structure of newly-formed zeolites) may interact (compete) with other cations present in solution and/or cations present in sorbent material (e.g. exchangeable cations in zeolite channels).

The removal efficiency of metal ions from aqueous solution strongly depended on the nature of sorbent material and the metal ion sorbed (Figure 7). In general, the removal efficiency for Zn^{2+} (15–81 % after 120 min) was higher than that for Ni^{2+} (0–65 % after 120 min), for all tested materials. These observations indicated higher affinity of zeolitic

materials for Zn^{2+} than for Ni^{2+} which was in line with published data showing higher sorption of Zn^{2+} than Ni^{2+} on zeolites (clinoptilolite and zeolite A) [35, 36]. According to some authors [36], the higher selectivity of zeolites for Zn^{2+} over Ni^{2+} can be related to the distinct ion electron configuration of these metals. Majdan et al. [36] showed that ions with d^5 (e.g. Mn^{2+}) and d^{10} (e.g. Zn^{2+}) electron configuration, owning weaker hydrolytic properties, interact strongly with zeolite framework and therefore their affinity to zeolite is much stronger than that for ions with d^8 (e.g. Ni^{2+}) electron configuration. The d^8 ions with stronger hydrolytic properties than those for the d^5 and d^{10} ions remain in aqueous solution in hydrated forms far from zeolite framework [36].

The highest removal efficiencies for Zn^{2+} after 120 min (80–81 %) were observed for 1-130-72, 5-70-72 and 13X. For the rest of tested materials, the Zn^{2+} removal efficiencies after 120 min gradually decreased in the following order: 1-190-6 (47 %) > CPT (28 %) > 5-190-6 (15 %). The highest removal efficiency for Ni^{2+} after 120 min (65 %) was observed for 13X. The rest of the studied materials had lower removal efficiency for Ni^{2+} after 120 min, i.e., 5-70-72 (44 %), 1-130-72 (32 %), CPT (21 %), 1-190-6 (10 %), 5-190-6 (0 %).

The observed differences in the removal efficiencies for metals can be due to the different physicochemical properties of the studied zeolites (e.g. different framework topology, chemical composition, surface properties, etc.). The results of previous studies showed that zeolites with lower Si/Al ratio and larger channel dimensions (e.g. zeolite X) should have better sorption performance for metals than zeolites with higher Si/
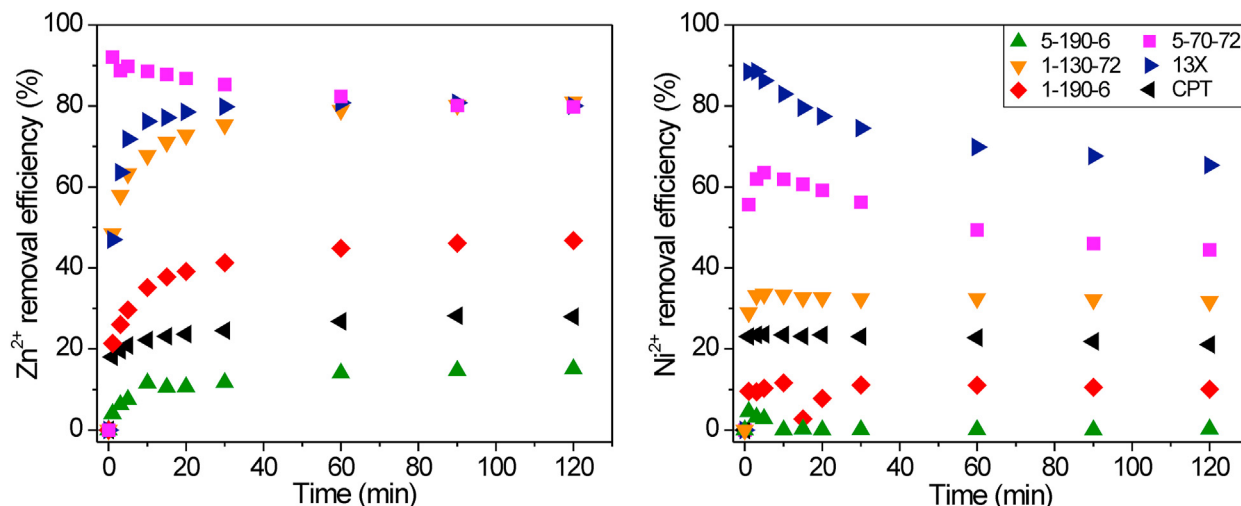

Figure 7. The removal efficiency for Zn^{2+} and Ni^{2+} using synthesized zeolitic materials and commercial sorbents at pH 5.

Al ratio and smaller channel dimensions (e.g. mordenite, clinoptilolite, analcime, phillipsite, chabazite) [35, 37, 38]. The greater the Al^{3+} substitution in the zeolite framework, the more cations (e.g. metals) are needed to maintain electrical neutrality, and hence, the higher the CEC. The channel dimensions, on the other hand, determine whether or not a given cation will fit into a particular zeolite framework.

The published data [35, 37, 38] were in line with our experimental results showing that the zeolite X rich material synthesized from PBM (5-70-72) and the commercial molecular sieve rich in zeolite X (13X) were the most effective sorbents for the removal of Zn^{2+} and Ni^{2+} from the aqueous solution. The relatively high zeolite X content for 5-70-72 (38 wt% of X, Table 5), low Si/Al ratio (Si/Al = 1.36, Table 2) and the large dimensions of zeolite X channels (three-dimensional pore system with 12-membered ring channels of 0.74×0.74 nm [39]) accounted for the high $CEC_{AmAcCorr}$ (261 ± 6 meq/100g), S_{BET} (313 m^2/g) and V_{micro} (0.145 cm^3/g) values of 5-70-72 (Table 3). The higher purity (higher zeolite X content) along with the lower Si/Al ratio (Si/Al = 1.08, Table 2) for the commercial molecular sieve 13X, led to the higher $CEC_{AmAcCorr}$ (344 ± 5 meq/100g), S_{BET} (585 m^2/g) and V_{micro} (0.289 cm^3/g) compared with those for the 5-70-72. Interestingly, the Zn^{2+} removal efficiency after 120 min for the 5-70-72 (80 %) was the same as that for the 13X (80 %) whereas the Ni^{2+} removal efficiency after 120 min for the 5-70-72 (44 %) was lower by 21 % compared with that for the 13X (65 %) (Figure 7).

Phillipsite rich material synthesized from PBM (1-130-72) showed also promising removal efficiency, especially for Zn^{2+}. Nevertheless, the phillipsite 1-130-72 had higher Si/Al ratio (Si/Al = 2.17, Table 2) and the smaller channel dimensions (three-dimensional pore system consisting of three intersecting 8-membered ring channels of 0.38×0.38 nm, 0.30×0.43 nm and 0.32×0.33 nm in the [100], [010] and [001] directions, respectively [39]) than the zeolite X. Such zeolite framework topology and crystal-chemistry caused cation exchange limitations which in turn resulted in the lower Zn^{2+} and Ni^{2+} sorption efficiency of phillipsite-bearing materials. On the other hand, the higher Si/Al ratio and the smaller channel dimensions of phillipsite were compensated, to some extent, by high amount of phillipsite in the synthesized material 1-130-72 (66 wt% of phillipsite, Table 5). This likely accounted for high Zn^{2+} removal efficiency of 1-130-72 after 120 min (81 %, Figure 7), comparable to that of zeolite X-bearing materials 5-70-72 and 13X (80 %, Figure 7). The Ni^{2+} removal efficiency for 1-130-72 after 120 min (32 %, Figure 7) was lower by 12–33 % than that for the zeolite X-bearing materials (13X and 5-70-72).

The analcime + phillipsite rich sample (1-190-6) exhibited significantly lower removal efficiency for both Zn^{2+} (47 %) and Ni^{2+} (10 %), compared with that of the phillipsite rich 1-130-72 (81 % for Zn^{2+} and 32 % for Ni^{2+}) (Figure 7). Although the 1-190-6 had relatively high total zeolite content (70 wt%, Table 5), its lower sorption performance for metal ions was attributed mainly to the lower amount of phillipsite and specific framework topology of analcime (pore system consisting of irregular channels formed by highly distorted 8-membered rings [39]). Analcime, which has a dense structure and non-intersecting channels exhibits at room temperature very limited ion exchange of its exchangeable cations for other cations [40]. In addition, analcime present in the sample 1-190-6 exhibited higher Si/Al ratio (Si/Al = 2.55, Table 2) what indicated its lower CEC, and thus the lower sorption performance in comparison with the zeolite X and phillipsite.

The natural clinoptilolite (CPT) exhibited relatively low removal efficiencies for Zn^{2+} (28 %) and Ni^{2+} (21 %) compared with the most of the studied samples (Figure 7). The lowest Zn^{2+} (15 %) and Ni^{2+} (0 %) removal efficiencies of all studied materials displayed the cancrinite rich sample 5-190-6 synthesized from PBM (Figure 7). The relatively low metal ions sorption efficiencies for CPT and 5-190-6, despite of their high total zeolite content (74–75 wt%, Table 5), may be related to clinoptilolite and cancrinite framework topology. Cancrinite has one-dimensional pore system consisting of 12-membered ring channels of 0.59×0.59 nm in the [001] direction [39]. The pore system of

clinoptilolite consists of two-dimensional pore system of alternating 8-membered and 10-membered ring channels of 0.41×0.47 nm and 0.44×0.72 nm in the [001] direction, respectively, interconnected with 8-membered ring channels of 0.40×0.55 nm in the [100] direction [39]. We believe that the lower dimensionality of cancrinite (one-dimensional) and clinoptilolite (two-dimensional) channel systems compared with that of phillipsite and zeolite X (both three-dimensional) may account to some extent, to the lower Zn^{2+} and Ni^{2+} removal efficiencies of the CPT and 5-190-6 materials. This conjecture was supported by published data showing that ion exchange kinetics within the zeolite structure depends on the number of channels and their spatial configuration; if all other factors remain equal, cations diffuse faster through zeolites with three-dimensional channel systems than those with one- or two-dimensional channel systems [40].

3.8. Sorption modeling

In order to better describe the metal sorption data, basic empirical modeling of the obtained data from kinetic and equilibrium experiments was performed. The kinetic data were modeled by the non-linear form of pseudo-first and pseudo-second order kinetics [22] (Fig. S5). The obtained values were used to determine the sorption rate since the simple empirical models are not suitable for the evaluation of the overall sorption mechanism, e.g., to differentiate between physical and chemical adsorption [41]. The experimental sorbed amounts at the equilibrium ($q_{e(exp)}$), calculated parameters (q_e, k_1, k_2) and correlation coefficients (R^2) are given in Table S2. Based on the course of individual curves, only selected data were suitable for kinetic modeling, i.e., nearly all data in the case of Zn^{2+} sorption (except the sample 5-70-72) and only data for the 1-130-72 in the case of Ni^{2+} sorption. The limiting factor was the initial desorption, which has been already discussed (see section 3.7.), and/or extremely fast reaching of the equilibrium (i.e. during the first time period). Based on the value of correlation coefficients, all data were better fitted by the pseudo-second order kinetics. The experimental sorbed amounts at the equilibrium corresponded well to the modeled values and to the already mentioned sorption efficiencies (see section 3.7.), where the relationship between the sorbed amount and the framework topology of individual zeolites was thoroughly described. Surprisingly, the highest sorption rate (i.e., the highest k_2 value) was observed for Zn^{2+} sorption on the natural clinoptilolite CPT despite its limited sorbed amount which may be related to fast occupation of more available sorption sites and their subsequent saturation. Subsequently, the sorption rate of Zn^{2+} on other zeolitic materials decreased in order: 1-130-72 $\approx$ 5-190-6 $\approx$ 13X > 1-190-6. Based on the results of Ni^{2+} sorption, only kinetic data for the phillipsite rich material 1-130-72 were sufficiently fitted by the kinetic models. The Ni^{2+} sorption rate was significantly higher compared to Zn^{2+} sorption on the 1-130-72 despite lower sorbed amount following the above-mentioned fast saturation of available sites (see the initial slope of curves in Fig. S5).

The equilibrium data were modeled by the non-linear form of Langmuir and Freundlich models [23, 24] (Fig. S6). The experimental sorbed amounts at equilibrium ($q_{e(exp)}$), calculated parameters ($q_{e(max)}$, K_L, K_F, n) and correlation coefficients (R^2) are given in Table S3. Based on the values of correlation coefficients, all data (except Zn^{2+} sorption on the analcime + phillipsite rich sample 1-190-6) were better fitted by Langmuir model (or the fitting was similar for both models). The modeled maximum sorbed amounts of Zn^{2+} on individual zeolites decreased in order: 5-70-72 > 1-130-72 > 13X > 1-190-6 > CPT > 5-190-6. However, slightly different order, i.e. 5-70-72 > 13X > CPT > 1-130-72 > 1-190-6, was observed for Ni^{2+} sorption. The obtained results for both metals showed the zeolite X rich sample synthesized from PBM (5-70-82), as the material with the highest sorption capacity. Contrarily, very limited (or even none) sorption was observed for the cancrinite rich material synthesized from PBM (5-190-6). The sorption affinity, that is given by the initial slope of the isotherm (K_L), showed the highest values for zeolite X rich materials (13X and 5-70-72) in the case of Zn^{2+} sorption and for
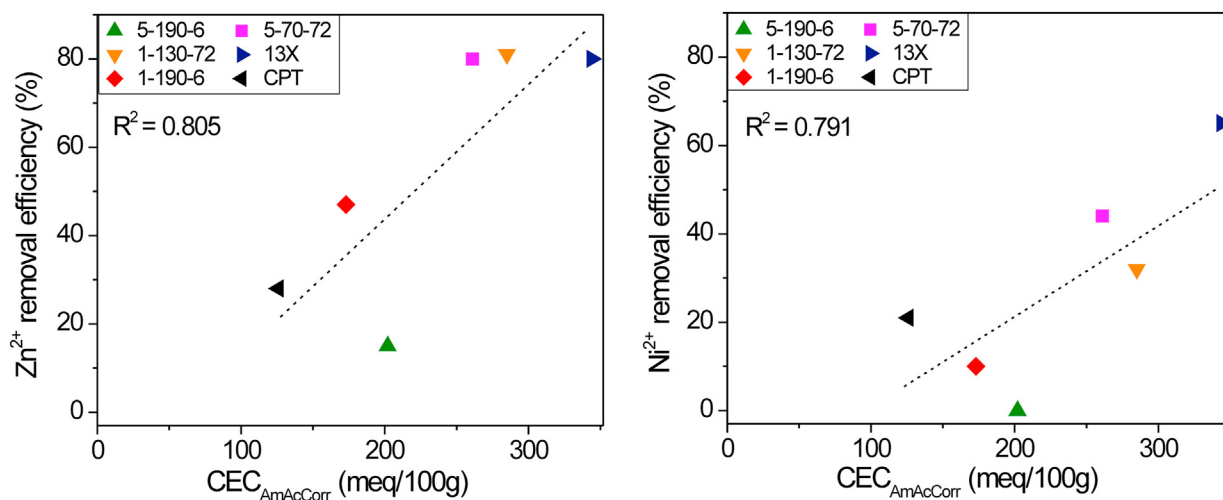
Figure 8. Zn^{2+} and Ni^{2+} removal efficiency plotted versus cation exchange capacity determined by ammonium acetate method corrected for the presence of non-exchangeable cations ($CEC_{AmAcCorr}$) for synthesized zeolitic materials and commercial sorbents.

phillipsite and analcime + phillipsite rich materials (1-130-72 and 1-190-6) in the case of Ni^{2+} sorption. The higher affinity of less effective materials in the case of Ni^{2+} sorption was probably caused by the preferential occupation of sites with higher affinity at lower Ni^{2+} concentrations and their subsequent fast saturation [42]. Nevertheless, this effect was not observed for Zn^{2+} sorption.

As mentioned in the previous chapter on the relationship between the sorption efficiency and the zeolite properties, the material rich in zeolite X showed the most promising results as the potential metal sorbent prepared from PBM. Phillipsite rich material synthesized from PBM showed also good sorption capacity against Zn^{2+} but this kind of material exhibited a lower maximum sorbed amount of Ni^{2+} compared to the samples rich in zeolite X and natural clinoptilolite.

3.9. Sorption mechanisms

Based on the literature [43, 44, 45, 46], the reduction in the concentrations of metals (e.g. Zn^{2+} and Ni^{2+}) in aqueous solutions after treatment with zeolitic sorbent materials can be related to: (i) cation exchange process between the metal cations present in aqueous solutions and exchangeable cations located in the channels within the zeolite framework, (ii) surface complexation on the zeolite surface sites (e.g. Al–OH or Si–OH) and/or (iii) precipitation of metals in aqueous solutions. In the present study, the pH value was controlled (pH = 5) for the entire duration of the kinetic and equilibrium sorption experiments to avoid metals precipitation and surface complexation. Since the surface complexation and precipitation pH for the most of metals (including Zn^{2+} and Ni^{2+}) is at pH > 6 [11,45,46], the cation exchange was likely the main mechanism of Zn^{2+} and Ni^{2+} sorption onto studied zeolitic materials at given experimental conditions. This assumption was supported by reasonable correlations between the removal efficiency of metal ions and $CEC_{AmAcCorr}$ values showing that the sorption of Zn^{2+} and Ni^{2+} from aqueous solutions increased with increasing cation exchange capacity of zeolitic materials (Figure 8). The cation exchange capacity of zeolites is generally related to the structural (also called constant or permanent) charge generated by non-equivalent isomorphous substitutions in the zeolite tetrahedra (usually Al^{3+} for Si^{4+}). The compensation of the negative permanent charge of zeolite framework via cation exchange was likely the main driving force of Zn^{2+} and Ni^{2+} removal from aqueous solutions using zeolitic sorbent materials. The obtain results showed that the zeolite framework topology (channels dimension and configuration) and the quantity of zeolite in the synthesized materials were the important parameters affecting the Zn^{2+} and Ni^{2+} removal efficiencies. The optimal synthesis conditions were determined as those when PBM was transformed into zeolite X (i.e. 5 M

NaOH, 70 °C and 72 h) because the synthesized material rich in zeolite X had the exceptional sorption performance mainly due to the large zeolite channel dimensions, low Si/Al ratio, high cation exchange capacity and high specific surface area. Thus, the zeolite X rich material seems to be the most promising sorbent material synthesized from PBM with possible application in water remediation processes.

4. Conclusions

Various zeolite-based sorbent materials (zeolite X, zeolite P, phillipsite, analcime, sodalite and cancrinite) with different sorption performance for studied metals (Zn^{2+} and Ni^{2+}) were synthesized from perlite-by product material (PBM) after interaction with NaOH solutions. Optimization of the synthesis procedure and detailed investigation of the zeolite products are necessary steps before large-scale application. The concentration of NaOH had significant impact on the type of synthesized zeolites whereas the reaction temperature and time influenced mainly the quantity of synthesized zeolite species. Zeolite X rich material exhibited the highest removal efficiency for both tested metals (Zn^{2+} and Ni^{2+}) from aqueous solutions. Phillipsite rich material showed also promising metal removal efficiencies, especially for Zn^{2+}. The lowest sorption efficiencies had cancrinite rich material. The amount of zeolite in the synthesized material and physicochemical properties of zeolites were the key factors affecting the metals removal. Zeolite with lower Si/Al ratio, higher cation exchange capacity, higher specific surface area and, in particular, with larger channel dimensions exhibited the highest Zn^{2+} and Ni^{2+} removal efficiency. Overall, the zeolite X material synthesized from PBM could be recommended as promising sorbent for metal cations. However, the efficiency and stability of this synthesized material should be tested under in-situ conditions prior to its application for remediation technologies.

Declarations

Author contribution statement

Data availability statement

Data will be made available on request.

Declaration of interest's statement

The authors declare no competing interests.

Additional information

Supplementary content related to this article has been published online at https://doi.org/10.1016/j.heliyon.2022.e12029.

References

[1] S. Šoltés, D. Kúšik, J. Mižák, Slovak Minerals Yearbook 2019, State Geological Institute of Dionyz Stur, Bratislava, 2020.

[2] U.S. Geological Survey, Mineral Commodity Summaries 2019, U.S. Geological Survey, 2019.

[3] G.E. Christidis, I. Paspaliaris, A. Kontopoulos, Zeolitisation of perlite fines: mineralogical characteristics of the end products and mobilization of chemical elements, Appl. Clay Sci. 15 (1999) 305–324.

[4] T.M. Mokgehle, W.M. Gitari, N.T. Tavengwa, Synthesis of di-carboxylic acid functionalized zeolites from coal fly ash for Cd(II) removal from acid mine drainage using column studies approach, J. Environ. Chem. Eng. 7 (2019), 103473.

[5] N. Moreno, X. Querol, C. Ayora, C.F. Pereira, M. Janssen-Jurkovicová, Utilization of zeolites synthesized from coal fly ash for the purification of acid mine waters, Environ. Sci. Technol. 35 (2001) 3526–3534.

[6] X. Ren, S. Liu, R. Qu, L. Xiao, P. Hu, H. Song, W. Wu, Ch. Zheng, X. Wu, X. Gao, Synthesis and characterization of single-phase submicron zeolite Y from coal fly ash and its potential application for acetone adsorption, Microporous Mesoporous Mater. 295 (2020), 109940.

[7] F. Collins, A. Rozhkovskaya, J.G. Outram, G.J. Millar, A critical review of waste resources, synthesis, and applications for Zeolite LTA, Microporous Mesoporous Mater. 291 (2020), 109667.

[8] I.V. Joseph, L. Tosheva, A.M. Doyle, Simultaneous removal of Cd(II), Co(II), Cu(II), Pb(II), and Zn(II) ions from aqueous solutions via adsorption on FAU-type zeolites prepared from coal fly ash, J. Environ. Chem. Eng. 8 (2020), 103895.

[9] Ch. Santasnachok, W. Kurniawan, H. Hinode, The use of synthesized zeolites from power plant rice husk ash obtained from Thailand as adsorbent for cadmium contamination removal from zinc mining, J. Environ. Chem. Eng. 3 (2015) 2115–2126.

[10] U.S. Environmental Protection Agency, Abandoned Mine Site Characterization and Clean up Handbook 2000, U.S. EPA, Seattle WA, 2000.

[11] W. Qiu, Y. Zheng, Removal of lead, copper, nickel, cobalt, and zinc from water by a cancrinite-type zeolite synthesized from fly ash, Chem. Eng. J. 145 (2009) 483–488.

[12] X. Querol, A. Alastuey, A. López-Soler, F. Plana, J.M. Andrés, R. Juan, P. Ferrer, C.R. Ruiz, A fast method for recycling fly ash: microwave-assisted zeolite synthesis, Environ. Sci. Technol. 31 (1997) 2527–2533.

[13] R. Sánchez-Hernández, A. López-Delgado, I. Padilla, R. Galindo, S. López-Andrés, One-step synthesis of NaP1, SOD and ANA from a hazardous aluminum solid waste, Microporous Mesoporous Mater. 226 (2016) 267–277.

[14] M. Osacký, H. Pálková, P. Hudec, A. Czímerová, D. Galusková, M. Vítková, Effect of alkaline synthesis conditions on mineralogy, chemistry and surface properties of phillipsite, P and X zeolitic materials prepared from fine powdered perlite by-product, Microporous Mesoporous Mater. 294 (2020), 109852.

[15] M. Król, W. Mozgawa, J. Morawska, W. Pichór, Spectroscopic investigation of hydrothermally synthesized zeolites from expanded perlite, Microporous Mesoporous Mater. 196 (2014) 216–222.

[16] S.E. Bailey, T.J. Olin, R.M. Bricka, D.D. Adrian, A review of potentially low-cost sorbents for heavy metals, Water Res. 33 (1999) 2469–2479.

[17] A. Dambrowski, Z. Hubicki, P. Podkościelny, E. Robens, Selective removal of the heavy metal ions from water and industrial wastewaters by ion-exchange method, Chemosphere 56 (2004) 91–106.

[18] M. Sprynskyy, B. Buszewski, A.T. Terzyk, J. Namieśnik, Study of the selection mechanism of heavy metal (Pb^{2+}, Cu^{2+}, Ni^{2+} and Cd^{2+}) adsorption on clinoptilolite, J. Colloid Interface Sci. 304 (2006) 21–28.

[19] M. Sasmaz, E.I.A. Topal, E. Obek, A. Sasmaz, The potential of Lemna gibba L. and Lemna minor L. to remove Cu, Pb, Zn and as in gallery water in mining area in Keban, Turkey, J. Environ. Manag. 163 (2015) 246–253.

[20] D.D. Eberl, User's Guide to RockJock – a Program for Determining Quantitative Mineralogy from Powder X-ray Diffraction Data, Open-File Report 03-78, U.S. Geological Survey, Boulder, Colorado, USA, 2003.

[21] A. Czímerová, J. Bujdák, R. Dohrmann, Traditional and novel methods for estimating the layer charge of smectites, Appl. Clay Sci. 34 (2006) 2–13.

[22] S.S. Gupta, K.G. Bhattacharyya, Kinetics of adsorption of metal ions on inorganic materials: a review, Adv. Colloid Interface Sci. 162 (2011) 39–58.

[23] K.Y. Foo, B.H. Hameed, Insights into the modeling of adsorption isotherm systems, Chem. Eng. J. 156 (2010) 2–10.

[24] G. Limousin, J.-P. Gaudet, L. Charlet, S. Szenknect, V. Barthès, M. Krimissa, Sorption isotherms: a review on physical bases, modeling, and measurement, Appl. Geochem. 22 (2007) 249–275.

[25] H. Shao, T.J. Pinnavaia, Synthesis and properties of nanoparticle forms saponite clay, cancrinite zeolite and phase mixture thereof, Microporous Mesoporous Mater. 133 (2010) 10–17.

[26] W. Mozgawa, The relation between structure and vibrational spectra of natural zeolites, J. Mol. Struct. 596 (2001) 129–137.

[27] S. Mintova, N.H. Olson, T. Bein, Electron microscopy reveals the nucleation mechanism of zeolite Y from precursor colloids, Angew. Chem. Int. Ed. 38 (1999) 3201–3204.

[28] G.D. Gatta, P. Cappelletti, N. Rotiroti, C. Slebodnick, R. Rinaldi, New insights into the crystal structure and crystal chemistry of the zeolite phillipsite, Am. Mineral. 94 (2009) 190–199.

[29] G.D. Gatta, F. Nestola, T.B. Ballaran, Elastic behavior, phase transition, and pressure induced structural evolution of analcime, Am. Mineral. 91 (2006) 568–578.

[30] F. Porcher, M. Souhassou, Y. Dusausoy, C. Lecomte, The crystal structure of a low-silica dehydrated NaX zeolite, Eur. J. Mineral 11 (1999) 333–344.

[31] K.F. Fischer, The crystal structure determination of the zeolite gismondite.CaAl2Si2O8.4H2O, Am. Mineral. 48 (1963) 664–672.

[32] I. Hassan, S.M. Antao, J.B. Parise, Sodalite: high-temperature structures obtained from synchrotron radiation and Rietveld refinements, Am. Mineral. 89 (2004) 359–364.

[33] I. Hassan, S.M. Antao, J.B. Parise, Cancrinite: crystal structure, phase transitions, and dehydration behavior with temperature, Am. Mineral. 91 (2006) 1117–1124.

[34] F. Rouquerol, J. Rouquerol, K. Sing, Adsorption by Powders and Porous Solids: Principles, Methodology and Application, Academic Press, San Diego, 1998.

[35] M.J. Zamzow, B.R. Eichbaum, K.R. Sandgren, D.E. Shanks, Removal of heavy metals and other cations from wastewater using zeolites, Separ. Sci. Technol. 25 (1990) 1555–1569.

[36] M. Majdan, S. Pikus, M. Kowalska-Ternes, A. Gladysz-Plaska, P. Staszczuk, L. Fuks, H. Skrzypek, Equilibrium study of selected divalent d-electron metals adsorption on A-type zeolite, J. Colloid Interface Sci. 262 (2003) 321–330.

[37] L.R. Rad, M. Anbia, Zeolite-based composites for the adsorption of toxic matters from water: a review, J. Environ. Chem. Eng. 9 (2021), 106088.

[38] G. Montégut, L. Michelin, J. Brendlé, B. Lebeau, J. Patarin, Ammonium and potassium removal from swine liquid manure using clinoptilolite, chabazite and faujasite zeolites, J. Environ. Manag. 167 (2016) 147–155.

[39] Ch. Baerlocher, L.B. McCusker, D.H. Olson, Atlas of Zeolite Framework Types, 6th revised edition, Elsevier, Amsterdam, 2007.

[40] R.T. Pabalan, F.P. Bertetti, Cation-exchange properties of natural zeolites, in: D.L. Bish, D.W. Ming (Eds.), Natural Zeolites: Occurrence, Properties, Applications, 45, Mineralogical Society of America, 2001, pp. 453–518. Reviews in Mineralogy and Geochemistry.

[41] J.-P. Simonin, On the comparison of pseudo-first order and pseudo-second order rate laws in the modeling of adsorption kinetics, Chem. Eng. J. 300 (2016) 254–263.

[42] M.R. Panuccio, A. Sorgonà, M. Rizzo, G. Cacco, Cadmium adsorption on vermiculite, zeolite and pumice: batch experimental studies, J. Environ. Manag. 167 (2009) 364–374.

[43] D.D. Shao, Q.H. Fan, J.X. Li, Z.W. Niu, W.S. Wu, Y.X. Chen, X.K. Wang, Removal of Eu(III) from aqueous solution using ZSM-5 zeolite, Microporous Mesoporous Mater. 123 (2009) 1–9.

[44] Y. Zhang, D.S. Alessi, N. Chen, M. Luo, W. Hao, Md.S. Alam, K.O. Konhauser, Y.S. Ok, A. Al-Tabbaa, Spectroscopic and modeling investigation of sorption of Pb(II) to ZSM-5 zeolites, ACS EST Water. 1 (2021) 108–116.

[45] M. Irannajad, H.K. Haghighi, E. Safarzadeh, Development of kinetic and equilibrium models for removal of Cd^{2+} and Zn^{2+} ions from aqueous solutions by clinoptilolite, Environ. Prog. Sustain. Energy 35 (2016) 633–641.

[46] S. Tahervand, M. Jalali, Sorption and desorption of potentially toxic metals (Cd, Cu, Ni and Zn) by soil amended with bentonite, calcite and zeolite as a function of pH, J. Cheochem. Explor. 181 (2017) 148–159.